Deep Learning-Based Quantification of Heat Gains and Impact on Building Energy Demand

Dongjun Mah[1,3]*, Hubo Cai[1], Kevin J. Kircher[2,3], Athanasios Tzempelikos[1,3]

[1]Purdue University, Lyles School of Civil Engineering,
550 Stadium Mall Dr., West Lafayette, IN, 47907, USA
Contact Information (dmah@purdue.edu, hubocai@purdue.edu)

[2]Purdue University, School of Mechanical Engineering,
550 Stadium Mall Dr., West Lafayette, IN, 47907, USA
Contact Information (kkirche@purdue.edu)

[3]Ray W. Herrick Laboratories, Center of High Performance Buildings,
140 S. Martin Jischke Dr., West Lafayette, IN, 47907, USA
Contact Information (ttzempel@purdue.edu)

* Corresponding Author

ABSTRACT

This paper introduces a novel approach for real-time monitoring of dynamic internal and solar heat gains using programmable low-cost cameras and deep learning techniques. A convolutional neural network (CNN)-based multi-head classification model was trained with High Dynamic Range (HDR) images, collected using a low-cost fisheye camera in a private office and fine-tuned using a separate dataset from an open-plan office. The results showed that the developed model could classify the status of multiple heat gains (occupants, equipment, lighting, windows) in predefined areas of the scene with great performance, achieving high precision and recall results. Furthermore, to evaluate the impact of real-time heat gain monitoring on energy demand, the large office space was modeled with energy simulation software using commonly assumed fixed heat gain schedules and real-time monitored dynamic schedules under the same weather conditions. The results showed that using fixed schedules may lead to significant errors, resulting in underestimation of some thermal load components and overestimation of others.

1. INTRODUCTION

HVAC control systems often rely on fixed setpoint schedules without heat gain information from occupancy, equipment usage, lighting, and windows. To optimize building operation, demand-driven HVAC control strategies have employed deep learning techniques to capture the dynamic energy demand of the building by detecting instantaneous heat gains. The emphasis in previous studies was placed on occupancy estimation (Choi, Um, Kang, Kim, & Kim, 2021b; Sayed, Himeur, & Bensaali, 2022; W. Zhang, Wu, & Calautit, 2022) using pretrained weights of a You Only Look Once (YOLO) (Redmon, Divvala, Girshick, & Farhadi, 2016) model. Equipment usage is another main source of internal heat gain in offices and (Wei, Tien, Wu, & Calautit, 2022) developed Faster Region-based CNN (R-CNN) (Ren, He, Girshick, & Sun, 2015) models for detecting occupant activity and computer monitor status. However, almost all of the previous studies focused on occupancy detection or the detection of single objects; for that purpose, they used high resolution images, which can cause privacy concerns, while typical cameras can be affected by sunlight because of limited color information capacity. Also, detection of window solar gains was not considered in previous demand-driven studies except (Donges, Morandi, Prada, Cappelletti, & Gasparella, 2024), which focused on object identification.

This work presents a CNN-based multi-head classification model to monitor major heat gain contributors (light dimming level, computers/monitors, windows, and occupancy) in real-time using a low-cost HDR image sensor. The model was trained using data collected in a private office and fine-tuned using a separate HDR image dataset collected

in an open-plan office, to evaluate transferability of the method. An energy model was also developed to evaluate the differences in energy demand with the monitored dynamic heat gain schedules vs using common fixed schedules.

2. TARGET OBJECT TYPES AND ROI GENERATION

A region of interest (ROI) program was developed to define the selected locations of interest (occupants, computers/monitors, electric lights, and shade position on the window). ROIs are manually selected from the captured representative images in the office to increase model performance, and flexibility and color-coded bounding boxes (Figure. 1) are generated for each object type to avoid confusion during selection. After selecting bounding boxes for each target type, the program internally saves their pixel location, used later for detailed status classification.

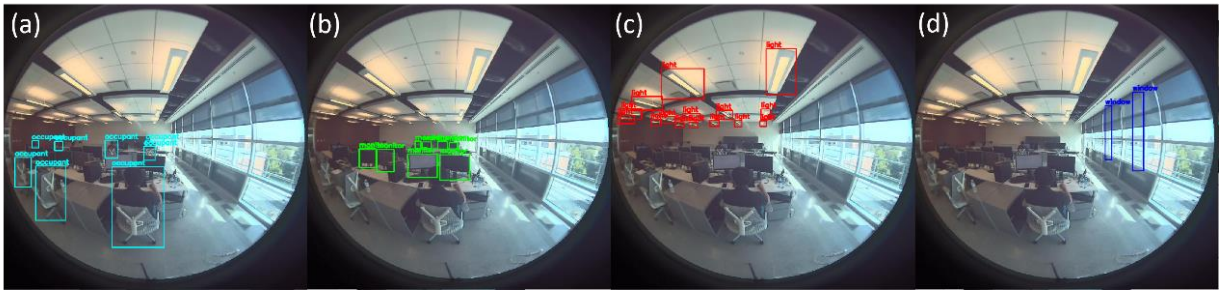

Figure 1: Representative examples of selected ROIs in the open-plan office:
(a): occupancy, (b): monitors, (c): electric lights, (d): shading position

3. DATASET USED FOR MODEL TRAINING

Two HDR image datasets were created for training the deep learning model and evaluate its ability to classify the status of selected objects. Data were first collected over 11 days in a private office (Figure. 2a) using two low-cost camera sensors with fisheye lens installed on one wall (at 1.5m and 1.8m from the floor) with 10 minute-intervals. Luminance conditions were changed by adjusting the shade position and light dimming levels (apart from naturally varying sky conditions) to generate a sufficient and balanced dataset with 1,078 HDR images (Figure. 2b) that include 9,702 selected areas with different status of object status levels.

A second dataset was collected over 15 days in an open-plan office (Figure. 2c) with larger luminance variability, using a sensor placed at 1.8m from the floor, to check transferable characteristics and flexibility of the model. 915 luminance maps were collected a (Figure. 2d) including 30,195 selected areas under different occupancy patterns (seated/vacant), electric lighting dimming levels (controlled in 10% intervals), multiple monitors (on/off), and window (shading position controlled in 10% intervals). For both datasets, a resolution of 330x330 was selected considering the computation load in the developed deep learning model, as well as the reliability of luminance maps for average luminance computation (Kruisselbrink, Dangol, & van Loenen, 2020).

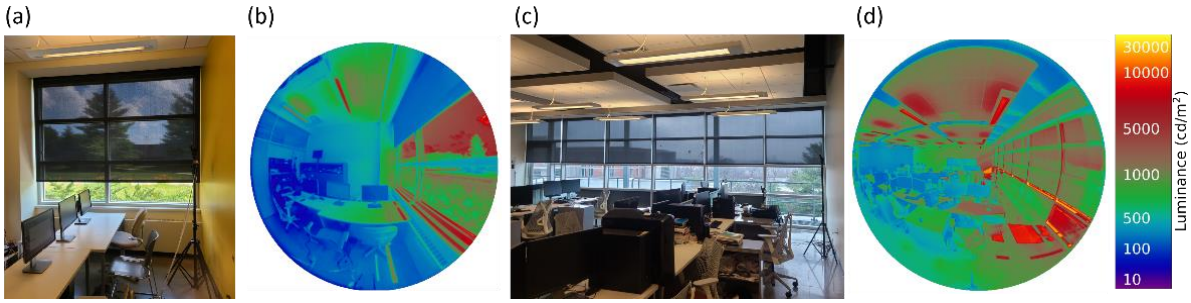

Figure 2: Private and open-plan office used for collecting data with installed cameras (a,c) and representative converted luminance maps (b,d)

4. CNN-BASED MULTI-HEAD CLASSIFICATION MODEL FOR HEAT GAIN MONITORING

4.1. Model architecture

The model architecture (Figure. 3) consists of four parts: feature extractor, self-attention module, feature cropper, and classification layers. The model first extracts proper information from each generated luminance map using feature extractor layers and increases the receptive field (condensed information area of input image in each feature pixel) of the extracted features using a self-attention module. Then, by rescaling coordinate information of the predefined area to extracted feature resolution, the model projects the monitoring area of interest directly to the extracted feature maps, to reduce the computational load. Finally, the cropped features input to classification layers to check status of occupancy, equipment usage, electric light dimming level, and shading position in the office.

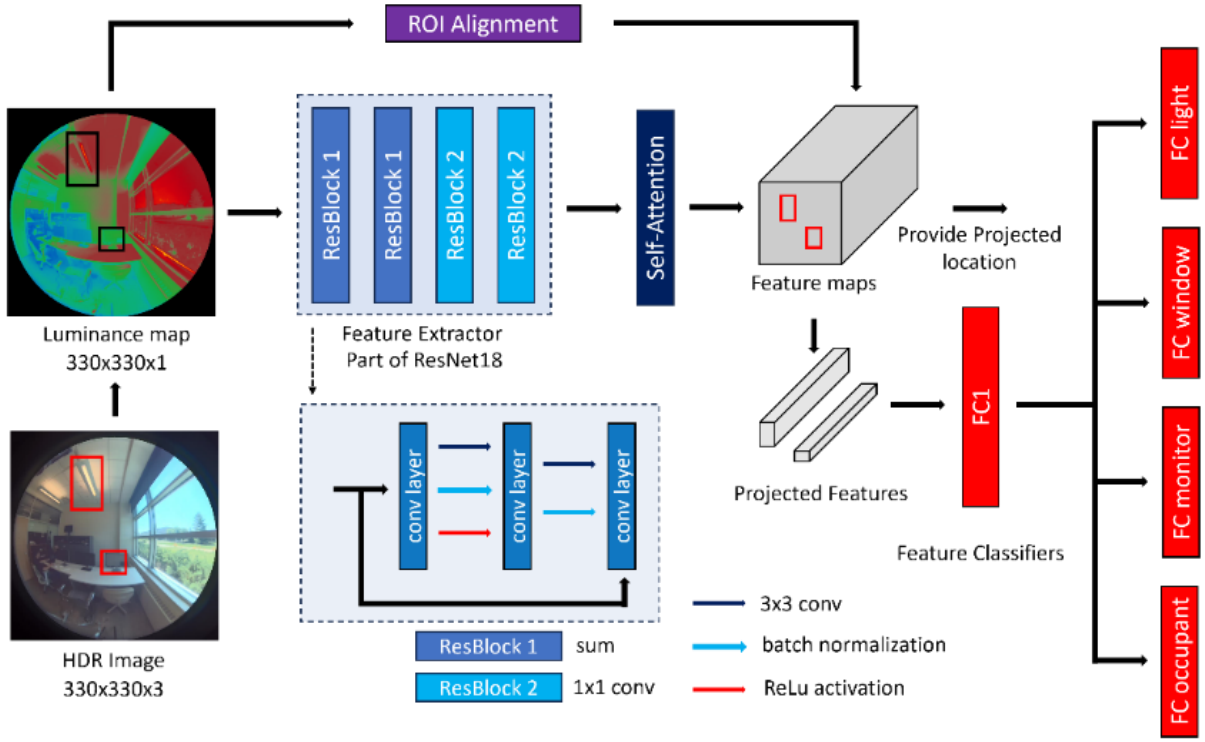

Figure 3: CNN model architecture

4.2. Model training and evaluation

For the private office dataset, 9 masked areas (3 occupant seats, 3 monitors, 2 electric lights, and 1 window area) in each image were used in each image (total 4,851 selected areas) during training. The dataset was randomly divided into 5 to 1 ratio to generate the training and test datasets. The training dataset was randomly divided into the same ratio again to generate the validation dataset. During training, weights in feature extractor modules (except the first layer) were not updated while the remaining layers (including self-attention layer and classifiers) were trained to balance computational efficiency and model performance.

In the open-plan office scenes, 33 masked areas (8 occupant seats, 8 monitors, 15 electric lights, and 2 window areas) were used in each HDR image (total 30,195 selected areas) during training. All the weights were transferred from the model trained with the private office dataset and the weights were updated during training except for the feature extractor weights. A combination of two binary cross entropy loss functions (for occupancy and equipment) and two 5-class cross entropy loss functions (for lighting dimming levels and shading position) was used:

$$Loss = L_{occupancy} + L_{euipment} + L_{light} + L_{window} \quad (1)$$

$$L_{occupancy}, L_{equipment}, L_{light}, L_{window} = -\frac{1}{N}\sum_{j=1}^{N}\left[\sum_{i=1}^{C} y_i \log(p_i)\right]_j \quad (2)$$

where y_i is the binary status label (e.g., on vs off condition, or 5-class approximate level label in Equation. 3), p_i is the softmax probability for the corresponding binary status or 5-class level, and N is the data size for each target set. A stochastic gradient decent algorithm with 0.9 momentum was used as optimizer with batch size of 16. In addition, 10^{-3} was used both for learning rate and for L2 regularization strength and 200 epochs were predefined for training the model. Since the lights and window status were divided into 5 classes in contrast to binary status of occupancy and equipment, macro-average precision and recall were computed. In addition, weighted average precision and recall results were monitored by considering the number of ROIs to evaluate the overall model performance with the training and validation datasets. The model performance was finally evaluated using precision and recall metrics of each classification result using the respective test datasets.

5. CNN MODEL PERFORMANCE RESULTS

The model showed good and stable classification performance (Figure 4) in precision and recall results for all four selected object types. The first layer of the feature extractor of the model (input luminance maps), self-attention module, and classification layers were well trained. The trained weights in these layers were transferred for training the model with the open-plan office dataset. Indeed, the model was also trained well in that case as well, classifying the status of selected objects with great accuracy (Figure 5). Additional epochs were required since the luminance patterns in the open-plan office presents higher variability. Overall, the results showed that the developed CNN-based multi-head classification model performs excellent in both cases, and that the developed method can be reliably used for real-time monitoring of internal and heat gain contributors in the offices.

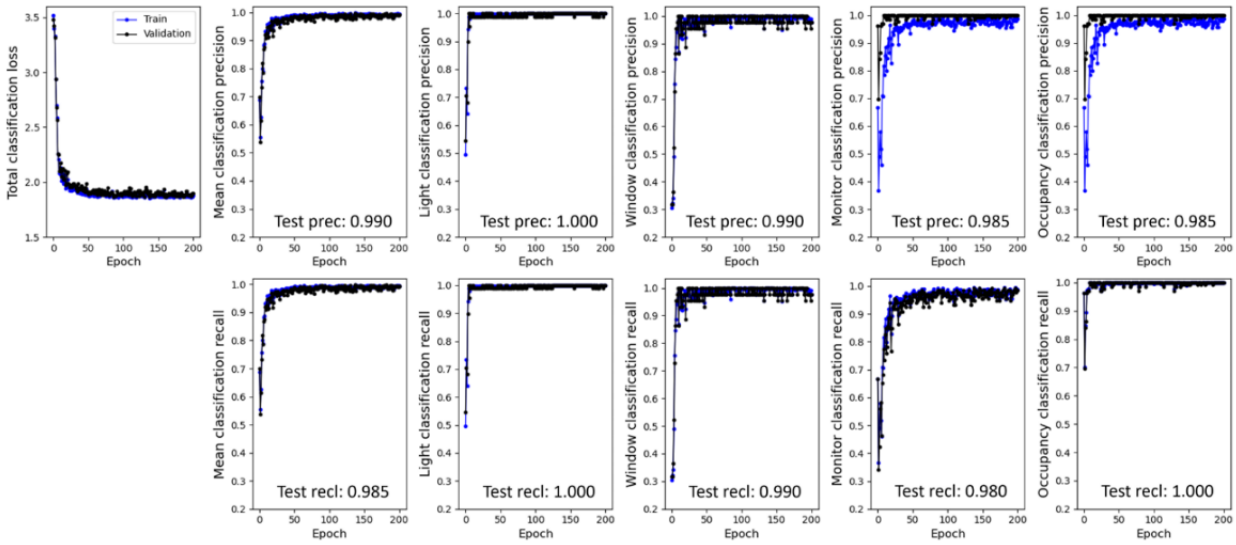

Figure 4: Total cross-entropy loss and overall and individual precision (top) and recall (bottom) results using the private office image dataset

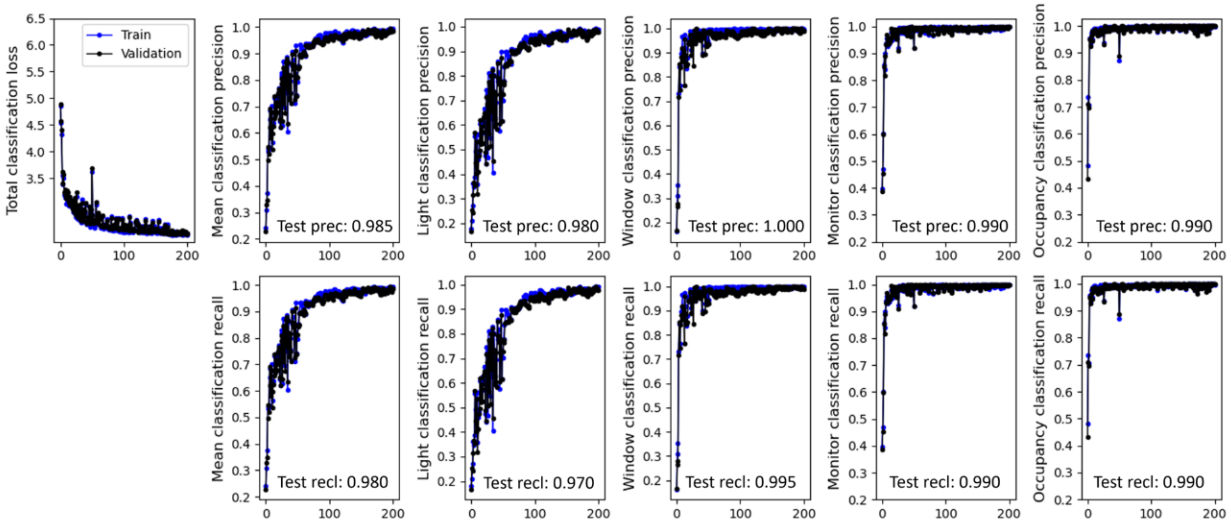

Figure 5: Total cross-entropy loss and overall and individual precision (top) and recall (bottom) results from using the open-plan office image dataset

6. IMPACT OF DYNAMIC HEAT GAINS MONITORING ON THERMAL LOAD AND ENERGY DEMAND

To evaluate the impact of real-time monitoring of internal and solar heat gains using the developed CNN model, the open plan office space, used for the experimental dataset collection, was modeled using EnergyPlus: the heat gains and energy demand computed with commonly used fixed schedules (baseline case) were compared with real-time monitored gains and computed energy demand under the same weather conditions. For the purpose of illustrating the results and comparing the computed energy demand of the office with fixed gains schedules, one representative sunny day in fall was selected (Sept. 21, 2023).

6.1. Simulation model geometry and material properties

The room geometry was first developed in 3D design software and was input to building energy simulation software; the office space (8m x 10m x 3.2m high) has south-facing windows (7.8m x 1.8m high) and is located in West Lafayette, Indiana (ASHRAE climatic zone 5A). An "ideal" HVAC system embedded in building energy simulation software was implemented to the model, and temperature setpoint schedules were assigned according to ASHRAE Standard 90.1 (ASHRAE., 2020) guidelines for weekdays (23.9°C for cooling with night setback at 26.7°C). Building construction material properties were assigned according to the construction plans: The overall thermal resistance of walls, floor, and roof was 4.8, 5.3 and 7.0 m^2K/W respectively. The windows were double-pane, air-filled with a listed U-factor of 1.48 W/m^2K (summer), and solar heat gain coefficient equal to 0.38. In addition, the window roller shades used in the actual office were included in the model with the following properties: 0.5mm thickness, 4% openness factor, 4% visible and solar transmittance and 75% exterior solar reflectance.

6.2. Baseline vs monitored heat gain schedules

The baseline schedules of occupancy, electric lighting, and equipment (computers and monitors) usage were generated using the recommended schedules in ASHRAE Standard 90.1 guide for the "office" space type during weekdays, for a fair comparison with the monitored dynamic gains case. These schedules are expressed as hourly percentages of maximum "capacity" for each type (occupancy, equipment usage, and lighting). The maximum occupancy in the office was set to 20 people, according to the floor area (and actual available workstations in the actual office). For equipment capacity, each occupant was assigned with one desktop computer and two monitors. Also, the baseline shade position was assumed fully open to mimic a building without automated shading control.

Dynamic schedules of occupancy, equipment usage, light dimming level, and shading position were generated by implementing the developed CNN-based monitoring model in the office space. In this case, the generated schedules contain the detailed dynamic status of the four heat gain components targets with 10 minute-intervals. The monitored

data showed that the real maximum occupancy was 8 people. This was then also linked to the maximum capacity of equipment usage in the space, both for the baseline and for the dynamic heat gains models, for a fair comparison.

When generating the dynamic equipment schedule, the captured status of occupancy and computer monitors were divided into two cases according to overlapping occurrence as shown in Figure (6). In addition, since the desktop computer cannot be directly captured because of its typical location (under the desk), its status was determined by checking the monitor status.

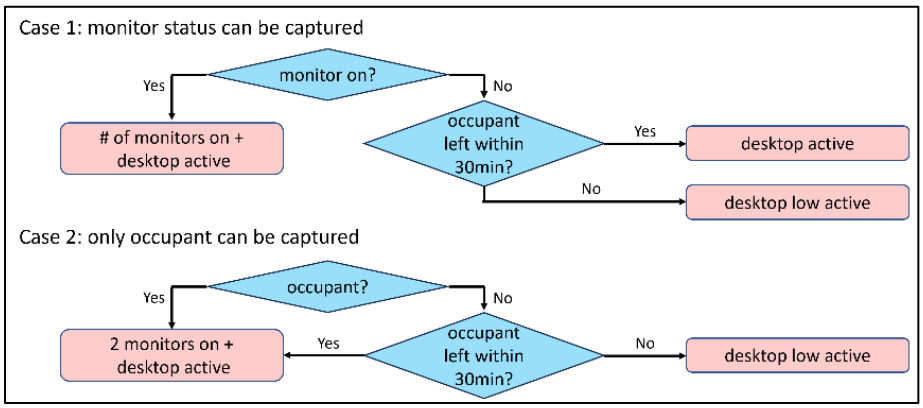

Figure 6: Decision criteria of equipment usage status

6.3. Baseline vs monitored internal and solar heat gain results and space energy demand

The heat gains contributions were then calculated by importing the generated schedule and the respective unit heat gain for each component in EnergyPlus, both for the baseline case (fixed schedules) and the real-time monitoring case. For people, 120W/person (including both sensible and latent heat gains) was used assuming typical moderate office activity. The installed lighting power density in the office was 10.1 W/m^2. Following the findings from (Menezes, Cripps, Buswell, Wright, & Bouchlaghem, 2014) in real offices, the heat gain from each high-end desktop was 150W when in active mode and 80W when in low active mode, and each monitor contributes 45W in the studied open-plan office. The hourly results for the selected representative day are presented in Figure (7).

The largest difference between the baseline and monitored heat gains results happens for occupants, since the actual monitored occupancy was much different from the assumed occupancy (Figure 7a). Partial occupancy (40%) happened for the entire time of monitoring, and this shows that capturing the status of occupants has a significant impact on heat gains estimation. In addition, occupancy is variable with time; during the evening, the monitored occupant gains were equal (or sometimes higher) than the assumed ones.

Although lighting operation is linked with occupancy (the space has an occupancy sensor and the baseline model has a matching schedule), the monitored lighting heat gains (Figure 7b) are not very different from the baseline results in the morning. From 12-4 pm, however, monitored lighting gains are lower than the baseline due to the actual detection of light dimming levels using the CNN classification model. In the evening, when people stayed later than the assumed baseline schedule, the monitored lighting gains are much higher than the commonly assumed ones. The equipment (monitors and desktop computers) heat gains were estimated properly by capturing monitors directly and linking equipment status with real occupancy. Although equipment gains were typically overestimated with fixed schedules, there were also instances of underestimation (Figure 7c), particularly when all occupants were simultaneously present. This is also due to the more accurate estimation of equipment gains using the values found in (Menezes et al., 2014).

The solar heat gain results (Figure 7d) were calculated directly by EnergyPlus. Similar to above, implementing the captured shading position schedule, covering most of the window during working hours, can reduce the amount of heat gain compared to the baseline case, especially if the shade solar reflectance is high. The opposite is also possible if a baseline case with shades always closed is considered.

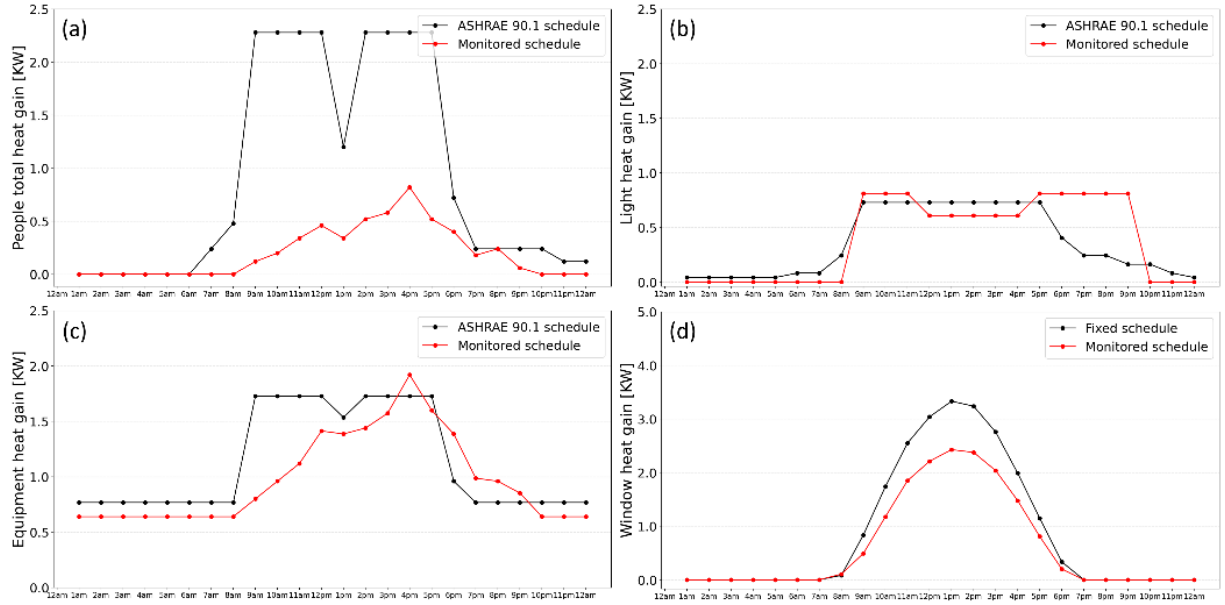

Figure 7: Real-time monitored internal and solar heat gains vs computed with commonly used fixed schedules (baseline) during the selected day in fall: heat gains from (a) people (b) lighting (c) equipment (d): windows.

The cooling load and energy demand of the studied office space were calculated using EnergyPlus with baseline fixed schedules and with dynamic schedules captured by the CNN-based monitoring model, for the selected day (under the same weather condition and keeping all other parameters the same). The software splits each gain in a convective and radiative portion, and these portions are used accordingly in the energy balance equations when calculating thermal loads. The realistic peak cooling load of the selected day calculated by monitoring dynamic schedules is 35% lower than the baseline case (Figure 8). Similarly, the total energy calculated by monitoring dynamic schedules is 31% lower than the baseline. The baseline model underestimated cooling load in the evening (when internal gains were captured with the CNN-based monitoring model). The cooling energy demand (load over time) results indicate that accurate detection and monitoring of heat gains, such as the method developed in this study, is important for any type of related demand-driven HVAC control.

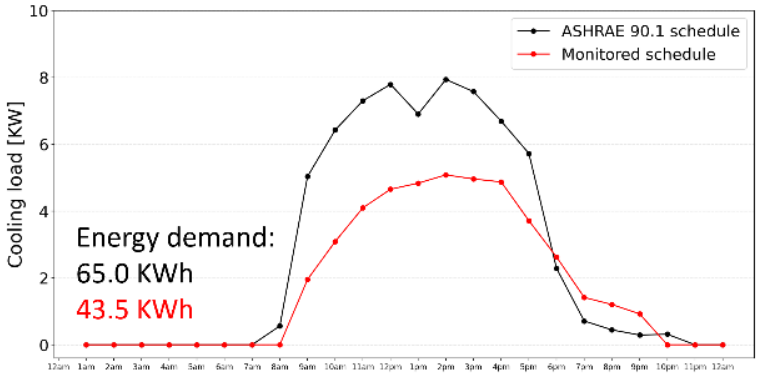

Figure 8: Hourly cooling load and energy demand with baseline fixed schedules and with dynamic schedules captured by the CNN-based monitoring model

8. CONCLUSIONS

This study shows that implementing real-time monitoring of dynamic internal and solar heat gains is important for accurate load estimation and related demand-driven HVAC control. A convolutional neural network (CNN)-based multi-head classification model was developed and trained with High Dynamic Range (HDR) images collected using a low-cost fisheye camera. The model was designed by combining transferred Resnet18 feature extractor, self-

attention module, feature cropper, and 4 classification layers for monitoring changes in occupancy, equipment, lighting, and window status in real time. The model was trained from scratch with the private office dataset to monitor the status of occupancy, equipment usage, electric lighting and windows. In addition, the transferability of the model was assessed by fine-tuning the trained model with the open-plan office dataset that included more complex scenes and various light dimming levels. Using precision and recall metrics, it was possible to check the great classification performance and the stabilized model performance in both private and open-plan office cases.

To evaluate the impact of real-time monitoring of heat gains on the thermal load of the open-plan office, the open plan office space used for the experimental dataset collection was modeled in EnergyPlus and evaluated (i) by importing commonly assumed fixed schedules and (ii) by importing the actual gains captured by the CNN-based monitoring model. The results showed that recommended fixed schedules may lead to significant errors in internal and solar gains and overestimation of internal/solar gains and cooling load. One of the main limitations in this work is the manually predefined areas of interest; future work might implement automated selection of ROIs using object detection and identification techniques. Also, in large offices, occupants face to various directions, making accurate detection of monitor status challenging. Multiple cameras with non-overlapping coverage areas can address this issue.

REFERENCES

ASHRAE. (2020). *ANSI/ASHRAE/IES Standard 90.1-2019: Energy Standard for Buildings Except Low-Rise Residential Buildings*. ASHRAE.

Choi, H., Um, C. Y., Kang, K., Kim, H., & Kim, T. (2021a). Application of vision-based occupancy counting method using deep learning and performance analysis. *Energy and Buildings*, *252*, 111389.

Choi, H., Um, C. Y., Kang, K., Kim, H., & Kim, T. (2021b). Review of vision-based occupant information sensing systems for occupant-centric control. *Building and Environment*, *203*, 108064.

Donges, J., Morandi, F., Prada, A., Cappelletti, F., & Gasparella, A. (2024). Occupants' interaction with building services: Development of a camera-based method for detailed monitoring of windows, shadings, and lights. *Building and Environment*, *248*, 111078.

File, M. (2015). Commercial buildings energy consumption survey (CBECS). *US Department of Energy: Washington, DC, USA*.

He, K., Gkioxari, G., Dollár, P., & Girshick, R. (2017). Mask r-cnn. *Proceedings of the IEEE International Conference on Computer Vision*, 2961–2969.

He, K., Zhang, X., Ren, S., & Sun, J. (2016). Deep residual learning for image recognition. *Proceedings of the IEEE Conference on Computer Vision and Pattern Recognition*, 770–778.

Kruisselbrink, T. W., Dangol, R., & van Loenen, E. J. (2020). Recommendations for long-term luminance distribution measurements: The spatial resolution. *Building and Environment*, *169*(June 2019), 106538. https://doi.org/10.1016/j.buildenv.2019.106538

Menezes, A. C., Cripps, A., Buswell, R. A., Wright, J., & Bouchlaghem, D. (2014). Estimating the energy consumption and power demand of small power equipment in office buildings. *Energy & Build.*, *75*, 199–209.

Redmon, J., Divvala, S., Girshick, R., & Farhadi, A. (2016). You only look once: Unified, real-time object detection. *Proceedings of the IEEE Conference on Computer Vision and Pattern Recognition*, 779–788.

Ren, S., He, K., Girshick, R., & Sun, J. (2015). Faster r-cnn: Towards real-time object detection with region proposal networks. *Advances in Neural Information Processing Systems*, *28*.

Sayed, A. N., Himeur, Y., & Bensaali, F. (2022). Deep and transfer learning for building occupancy detection: A review and comparative analysis. *Engineering Applications of Artificial Intelligence*, *115*, 105254.

Wei, S., Tien, P. W., Wu, Y., & Calautit, J. K. (2022). A coupled deep learning-based internal heat gains detection and prediction method for energy-efficient office building operation. *Journal of Building Eng.*, *47*, 103778.

Zhang, H., Goodfellow, I., Metaxas, D., & Odena, A. (2019). Self-attention generative adversarial networks. *International Conference on Machine Learning*, 7354–7363. PMLR.

Zhang, W., Wu, Y., & Calautit, J. K. (2022). A review on occupancy prediction through machine learning for enhancing energy efficiency, air quality and thermal comfort in the built environment. *Renewable and Sustainable Energy Reviews*, *167*, 112704.

ACKNOWLEDGEMENT

The authors would like to thank the Center for High Performance Buildings at the Ray W. Herrick Laboratories and the Lyles School of Civil Engineering at Purdue for the financial support.